OPEN ACCESS

University of BRISTOL

Peer reviewed version

Link to published version (if available):
10.1088/0964-1726/25/8/085008

Link to publication record in Explore Bristol Research
PDF-document

University of Bristol - Explore Bristol Research
General rights

MORPHING HYBRID HONEYCOMB (MOHYCOMB) WITH IN-SITU POISSON'S RATIO MODULATION

Callum J. C. Heath*, Robin M. Neville, Fabrizio Scarpa, Ian P. Bond & Kevin D. Potter

Advanced Composites Centre for Innovation and Science (ACCIS),
Department of Aerospace Engineering, University of Bristol, Queen's Building,
University Walk, Bristol BS8 1TR, UNITED KINGDOM
*Email: c.heath@bristol.ac.uk , web page: http://www.accismultifunctional.com/

ABSTRACT

Electrostatic adhesion can be used as a means of reversible attachment. Through application of high voltage (~2kV) across closely spaced parallel plate electrodes, significant shear stresses (11 kPa) can be generated. The highest levels of electrostatic holding force can be achieved through close contact of connection surfaces; this is facilitated by flexible electrodes which can conform to reduce air gaps. Cellular structures are comprised of thin walled elements, making them ideal host structures for electrostatic adhesive elements. The reversible adhesion provides control of the internal connectivity of the cellular structure, and determines the effective cell geometry. This would offer variable stiffness and control of the effective Poisson's ratio of the global cellular array. Using copper-polyimide thin film laminates and PVDF thin film dielectrics, double lap shear electrostatic adhesive elements have been introduced to a cellular geometry. By activating different groups of reversible adhesive interfaces, the cellular array can assume four different cell configurations. A maximum stiffness modulation of 450 % between the "All off" and "All on" cell morphologies has been demonstrated. This structure is also capable of in-situ effective Poisson's ratio variations, with the ability to switch between values of -0.45 and 0.54. Such a structure offers the potential for tuneable vibration absorption (due to its variable stiffness properties), or as a smart honeycomb with controllable curvature and is termed MOHYCOMB (MOrphing HYbrid honeyCOMB).

1   INTRODUCTION

Electrostatic adhesion can provide reversible attachment within host structures. Closely spaced electrodes experience Coulomb attraction when subject to a large potential difference. With sufficiently close contact, significant holding forces can be generated which, when combined with reasonable friction between adjacent surfaces, can enable the transfer of increased shear stress across otherwise separate structural entities. This provides the potential to control the load path within a structure.

Cellular structures represent a promising host structure for such functional elements for two primary reasons. Firstly, the individual local elements of a cellular structure are usually relatively low stiffness. This conformability theoretically allows for closer contact to be generated between adjacent electrode elements in an electrostatic adhesive setup, as the electrodes can overcome large scale surface waviness. Secondly, the use of a large array structure allows for the introduction of numerous electrostatic adhesive interfaces, and thus a multitude of potential load paths through the structure.

This study considers the introduction of electrostatic adhesive elements within a host cellular structure (Figure 1), in order to control the effective geometry of the constituent cells. Electrostatic adhesive joints are introduced into the cell walls of a honeycomb (Figure 1). When a high voltage (~2kV) is applied across the joints, the electrodes adhere and allow load transfer across the cell wall. Non-activated joints slip and do not transfer loads. Thus, the attachment of individual members of the larger array can be controlled. Using this method, several effective cell geometries are investigated, both in terms of the induced effective global stiffness of the array, and the achievable effective Poisson's ratio control. Figure 2 shows four example configurations from the multitude possible, and the unit cells used for Poisson's ratio calculations.

2   BACKGROUND

To the best of the Authors' knowledge, the use of electrostatic adhesive elements for a variable stiffness cellular structure is a novel concept. The use of electrostatic adhesion in variable stiffness structures, and the concept of effective Poisson's ratio manipulation of cellular structures are considered herein.

Previous studies have considered the introduction of electrostatic adhesive elements to host structures in order to modulate the stiffness and response of the host, with much of the focus resting on the concept of Electro-Bonded Laminates (EBL). Tabatha *et al* demonstrated a variable stiffness concept whereby the bending resistance of a layered structure of thin polyimide between nickel electrodes could be increased through the application of a high voltage [1]. Bergamini *et al* provided significant extension to this concept, whereby permanent adhesive layers within composite beam structures, both monolithic and sandwich structures, were replaced by reversible electrostatic bonding [2–4]. The application of a large potential difference across the integrated electrodes generated a significant holding force, allowing for increased shear stress transfer across the electroadhesive interface, thereby increasing the global bending stiffness of the structure. Heath *et al* investigated the operation of these devices under higher applied loading, demonstrating improved functionality from a fabrication method which resulted in closer electrode spacing [5]. From the work of Di Lillo *et al,* the high levels of achievable holding force are clear, particularly for less rigid electrode elements [6]. Raither *et al* considered some other uses of these thin film electroadhesive devices within larger structures, utilising the devices for the opening and closing of discrete bays of an aerofoil section to confer variations in the torsional stiffness of the section, and thus the lift/drag response of the aerofoil [7,8]. This study considers the introduction of electrostatic adhesive elements in a lower level of the overall structural hierarchy, within the elements of a cellular core structure.

In 1987 Lakes reported one of the first cellular structures with negative Poisson's ratio [9]. He identified that the negative Poisson's ratio (NPR) was caused by the re-entrant 3D topology of the cells. In subsequent work, Lakes also identified some other examples of NPR and various mechanisms behind them [10]. For honeycombs, the most important effect of the Poisson's ratio is the bending behaviour. Poisson's ratio effects cause synclastic or anticlastic curvatures depending on the value of Poisson's ratio [11] (Figure 3). Evans also first coined the term "auxetic" for referring to NPR materials [12].

The effect of the Poisson's ratio on the bending behaviour of a honeycomb is a serious manufacturing concern for sandwich panels. Manufacturing a dome-shaped component from a positive Poisson's ratio honeycomb necessitates suppressing the natural curvature of the honeycomb, which results in local buckling or crushing of the cell walls [11]. The Poisson's ratio of a honeycomb can be controlled by tailoring the shape of the honeycomb unit cell. The most common honeycomb geometry is the regular hexagon, which is common to most commercially available honeycombs because of the manufacturing process

consisting of an expanding stack of laminated sheets [13]. The hexagonal geometry has an in-plane Poisson's ratio close to 1 [14]. Honeycombs with re-entrant hexagonal cells [15] or chiral geometry [16] both have Poisson's ratio of –1. A zero-Poisson's ratio (ZPR) honeycomb is a particular subset of cellular structures that shows no secondary curvature when bending around one axis. Several ZPR honeycomb concepts have been recently proposed. Grima *et al* have described a honeycomb made of cells with one re-entrant and another outward-facing side [17,18]. Olympio and Gandhi have proposed a honeycomb with a mixture of regular hexagons and re-entrant hexagon cells [19,20], while Scarpa *et al* have produced a honeycomb with a crossed zigzag pattern [21–25]. All of these ZPR honeycombs achieve ZPR through a balance of re-entrant and non-re-entrant features. Recent novel advances of ZPR honeycombs has demonstrated their increasing potential for morphing applications [26,27].

A controllable and reversible means of attachment is needed to switch between the different cellular configurations. Electrostatic adhesion can provide such an attachment, although this requires that the generated holding strength is sufficiently large. For closely spaced electrodes of the geometries considered herein, the primary electrostatic force generated is perpendicular to the electrode surfaces. For the simple configuration shown in Figure 4 (a), the electrostatic normal strength of each interface can be evaluated as:

$$\sigma_N = \frac{\varepsilon_0 \varepsilon_r U^2}{2d^2} \qquad\qquad 1$$

In Equation 1. ε_0 is the permittivity of free space (8.854×10^{-12} Fm^{-1}), ε_r is the relative permittivity of the dielectric layer, U is the potential difference between the electrodes and d is the electrode separation. In reality, however, the electrode surfaces are not in intimate contact, and thus an air gap is present between the contact surfaces (Figure 4). To account for the introduction of an air gap, the configuration can be more accurately represented as in Figure 4 (b). The inclusion of a region of lower permittivity leads to a reduction in the achieved holding force, and a better approximation for this force has been shown by Mao *et al* [28]:

$$\sigma_N = \frac{\varepsilon_0 \varepsilon_{r1} \varepsilon_{r2}^2 U^2}{2(\varepsilon_{r1} d_2 + \varepsilon_{r2} d_1)^2} \qquad\qquad 2$$

The new parameters included in Equation 2 are the relative permittivity of the dielectric layer ε_{r1}, the relative permittivity of the air gap layer ε_{r2}, and the thicknesses of the dielectric and air gap layers respectively (d_1 and d_2). As aforementioned, the electrostatic force generated is normal to the electrode surfaces, but the double lap shear joints within the cellular structure require shear stress transfer. The shear strength can be approximated as the product of the normal strength from Equation 2 and the coefficient of friction at the interface μ. Using Equation 2, and considering parameters similar to those used by Heath *et al*, estimates for normal strengths and shear tractions for electrostatic adhesive devices are shown in Table 1. The dielectric properties were calculated based on the assumption of using a Polyvinyl Fluoride (PVF) film (TWH20BS3 Tedlar, Du Pont, USA).

3   DESIGN AND FABRICATION

Given the novelty of this concept, a relatively simple design was chosen for the overall cellular host structure. The fabrication method was also relatively simplistic, and allowed for the rapid production of a functional prototype. As this technology is developed, more advanced materials and processes could be introduced to enhance the design.

The initial proof-of-concept prototype was intended to allow for a clear demonstration of both the variable stiffness and variable Poisson's Ratio behaviour of the electrostatic cellular structure. The initial design has a larger cell geometry than the one typical of a cellular core in a composite sandwich structure, with unit cell dimensions as given in Table 2. Parameter b represents the electrode overlap length.

A thin film laminate of 25 μm polyimide and 35 μm electrodeposited copper was used as the electrode material. The copper serves as the conductive electrode element whilst the polyimide backing provides the insulation between the high voltage element and the rest of the host structure. The dielectric chosen was a thin film PVF known as Tedlar TWH20BS3 (Du Pont, USA). With an estimated dielectric strength of 7kV for the supplied thickness of 50 μm, a relative permittivity of 11 and a friction coefficient of 0.2, the PVF seemed an appropriate choice of dielectric to achieve a reasonable electrostatic holding force [29].

The primary cellular structure was constructed using 285.95 GSM paper card, and was produced as 4 separate column elements (Figure 6). Electrode elements were bonded to the host card using double sided adhesive tape, and electrical connections between elements across the array were integrated by means of a copper tape with a conductive adhesive. The dielectric layer was bonded to the host structure on one side of each electrostatic interface. The bonding was carried out in such a manner that there was no additional adhesive layer between the copper electrode surface and the dielectric layer, so that additional surface separations were not induced. A heavy metal cylinder was used to roll the copper electrodes after bonding to the host card structure, helping to ensure smooth external electrode surfaces and to minimise the spacing of the air gaps.

In order to load the cellular structure, end tabs were produced from a polylactic acid (PLA) blend by using an additive layer manufacture (ALM) process. The end tabs help to maintain the initial cell shape prior to each test and were designed to be sufficiently stiff to transmit all loads to the cellular structure (Figure 7).

Materials testing was carried out to quantify the elastic modulus for the card host material with a 1 kN load cell connected to an INSTRON 8433 test machine. Using the standard ASTM D882-12, from tensile tests of 7 samples at a testing rate of 25 mm/min, the average modulus of elasticity was found to be 2.834 ± 0.157 GPa. The nominal dimensions of these test samples was a gauge length of 254 mm, a width of 25 mm, and a thickness of 0.35 mm.

The in-plane Poisson's ratio of a honeycomb based on the assumption that the cells deform primarily by bending of the cell walls, with negligible axial and shear deformations can be calculated following Gibson and Ashby's approach [14]:

$$\nu_{xy} = \frac{h/l \sin\theta + \sin^2\theta}{\cos^2\theta} \qquad 3$$

The other in-plane Poisson's ratio (ν_{yx}) is $1/\nu_{xy}$. Substituting in the dimensions shown in Figure 2 and Table 2 the Poisson's ratios for the regular and re-entrant configurations are obtained as indicated in Table 3. Large changes in Poisson's ratio are theoretically possible if the structure can switch between regular hexagonal and re-entrant hexagonal cell shapes.

4   EXPERIMENTAL

A basic double lap shear test was carried out to establish the shear holding strength of the integrated electrostatic interface joints. For these tests a 1 kN load cell connected to an INSTRON 8433 test machine was used, with an extension rate of 1 mm/min. Electrode contact areas were 900 mm² (30 x 30 mm square), and ten repeat tests were carried out at each voltage (1, 2, 3 kV). Two primary test types were carried out to assess the performance of the MOHYCOMB. Firstly, direct tension and compression tests were carried out on the entire MOHYCOMB structure, with a nominal height (y) of 140 mm, a width (x) of 130 mm and a depth (z) of 30 mm. With a chosen displacement rate of 10 mm/min, over ten repeat tests for each arrangement, the load-displacement behaviour of the cellular structure in each of the four configurations can be established. From this testing the global stiffness of the structure can be ascertained and along with the variation in mechanical properties provided by the electrostatic adhesive elements. Secondly, the INSTRON was used to extend the cellular structure by a known displacement of 4 mm, while an Imetrum video gauge system was used to track the motion of a number of vertices. This test was repeated for the regular, re-entrant, and all-on configurations (Figure 2), thus enabling a comparison of the Poisson's contraction for each configuration. Figure 8 shows the section of honeycomb tracked by the video gauge, and the virtual representation generated from the tracked vertices' XY coordinates.

A high voltage supply is necessary to enable the electroadhesive devices to provide a means of reversible attachment. A high voltage DC-DC step up convertor (commercially available EMCO *F Series*, EMCO High Voltage Corporation, USA) was used for this purpose. A potential divider was also incorporated to monitor the output voltage.

5   RESULTS

From the double lap shear tests, the electrostatic interface strengths have been established for a range of applied voltage values. Ten repeat tensile tests of the double lap shear joint were carried out, and the average maximum shear load carried by the joint for each voltage was established. Figure 9 shows the values found along with a comparison to those values expected using Eq. 2, assuming an air gap of 3.5 μm (from previous research [5]. Recall that the double lap shear joint allows for the integration of two discrete electrostatic adhesive interfaces, doubling the electrode contact area.

There appears to be a relatively close match between the observed results and those calculated from Eq. 2. Assuming the loading on the integrated electrostatic adhesive elements is for the most part planar, each element can carry around 10 N in tension before failure when subjected to a potential difference of 2 kV. The total shear stress transferred by each joint is thus equivalent to approximately 11 kPa. The joints fail by means of slip once the local stress exceeds the critical shear stress level, determined by the critical electrostatic holding force. The holding mechanism can re-engage after slip if the shear stress at the interface falls below the critical value, provided that close contact between the adjacent electrodes is maintained.

One of the key objectives of the integrated electrostatic adhesive elements was to provide variable stiffness functionality to the cellular structure. The stiffness of each configuration was thus investigated. From the load extension curves it is clear that the "All on" configuration demonstrates the highest effective stiffness, under both tensile and compressive loading, followed by the re-entrant, regular, and "All off" configurations respectively (Figure 10). This is expected behaviour, as this is the order of greatest to fewest cells (effective density) and highest to lowest total linkages. The imparted potential difference (if any) was 2 kV.

In order to provide a quantitative comparison the axial stiffness (in the Y-direction) of each cellular configuration, linear curve approximations were added to each Load-Extension data set. The gradient of each provides a reasonable, albeit rudimentary, comparison between each configuration. These values show that large controllable variations in stiffness of the honeycomb structure can be achieved through voltage application across chosen selections of electrostatic adhesive joints. Table 4 highlights the extent of the functional potential, with a 450 % stiffness change possible between the "All off" and "All on" configurations (in tension). The tensile response of the cellular structures is likely to be more repeatable due to the buckling observed in the honeycomb during the compressive testing. The data show that an electrostatically reconfigurable variable stiffness cellular structure can be designed and produced.

Figure 11 shows the regular and re-entrant configurations at the beginning and end of the test. A difference in Poisson's ratio can already be observed; the regular configuration contracts laterally, while the re-entrant configuration expands in the transverse direction. The Poisson's ratios are calculated as follows. For a given level of imposed displacement along the y direction, a bounding box is generated by extracting the minimum and maximum X and Y coordinates of the vertices. This box is treated as the area of the honeycomb. This procedure is repeated for every frame of the video gauge data. By comparing the dimensions of the bounding boxes from two frames (in this case for $\Delta y = 0$ mm and $\Delta y = 10$ mm) the deformations $(\Delta x, \Delta y)$, strains (ϵ_x, ϵ_y), and Poisson's ratios (ν_{xy}, ν_{yx}) can be calculated. These results are shown in Table 5.

From Table 5 it is clear that significant changes in the Poisson's ratio can be achieved depending on the selection of electrostatic interfaces that are activated. The regular configuration demonstrates positive Poisson's ratios, whilst the re-entrant hexagonal topology shows an auxetic behaviour. This variation is significant and, therefore, demonstrates the in-situ Poisson's ratio control introduced by the use of electrostatic adhesive devices. Comparing the observed Poisson's ratios to those expected from the theoretical analysis, there is some significant variation. During the deformation of the structure under loading it was noticed that a number of the electrostatic adhesive joints that were activated still displayed some significant slippage. The theoretical Poisson's values are determined assuming a consistent and known cell morphology and linkage connectivity. If slippage occurs on a large proportion of the electrostatic adhesive joints, then the cellular shape cannot be determined to be a regular hexagon and, therefore, one would expect a larger deviation from the theoretical Poisson's ratio value due to the invalidity of the assumptions. In addition to this, some electroadhesive joints appeared to remain engaged despite being apparently disconnected from the high voltage supply. Such joints were able to transfer shear stress, at least to a certain level, and thus influence the apparent cellular morphology and the resulting mechanical response of the global structure. These joints likely remained engaged due to the residual charge from earlier tests, despite the best efforts to fully discharge these electrodes. The first issue related to premature joint slippage was observed for the shorter horizontal electrostatic joints, and the issue of unintentional sticking for the larger horizontal members. These two effects were predominantly observed for the regular configuration, as shown in Figure 12. There is, therefore, a clear requirement to improve the controllability and robustness of the individual electrostatic adhesive joints, in order to demonstrate a larger range of Poisson's ratio modulation.

6   CONCLUSIONS

In this study, a novel cellular structure with electrostatically tuneable stiffness and in-situ Poisson's ratio has been demonstrated. The application of high voltage across integrated electrostatic adhesive interfaces

allows for the control of load path and cell shape of the cellular structure. The integrated electrostatic adhesive interfaces can resist approximately 11 kPa shear stress when subject to a potential difference of 2 kV, allowing for reasonable load transfer through the joints when enabled. The prototype has given a clear demonstration of a 450 % stiffness variation between the "All off" and "All on" configurations. In addition, the ability to provide a significant shift in the effective Poisson's ratio of the cellular structure through a controlled switch between the regular and re-entrant configurations has been shown. The overall concept of the use of electrostatic adhesive elements within a cellular structure is, to the best of the authors' knowledge, a novel one. The demonstration of resulting functionality highlights the value of this technology, and there exists significant potential for larger scale cellular structures with variable stiffness and Poisson's behaviour.

7   RESEARCH EXTENSIONS

Further work will focus on potential applications of this technology. Control of the resulting curvature of such a honeycomb when subject to out-of-plane loading would be a clear next step for this research. Refinements to the integration of the electrostatic elements, particularly in terms of reliability, durability and manufacturing complexity would be of significant value in the further development of the concept. Dielectric enhancements could provide increased electrostatic holding force, either increasing the operational envelope of such structures, or allowing for reductions in voltage application, increasing robustness and reducing power requirements.
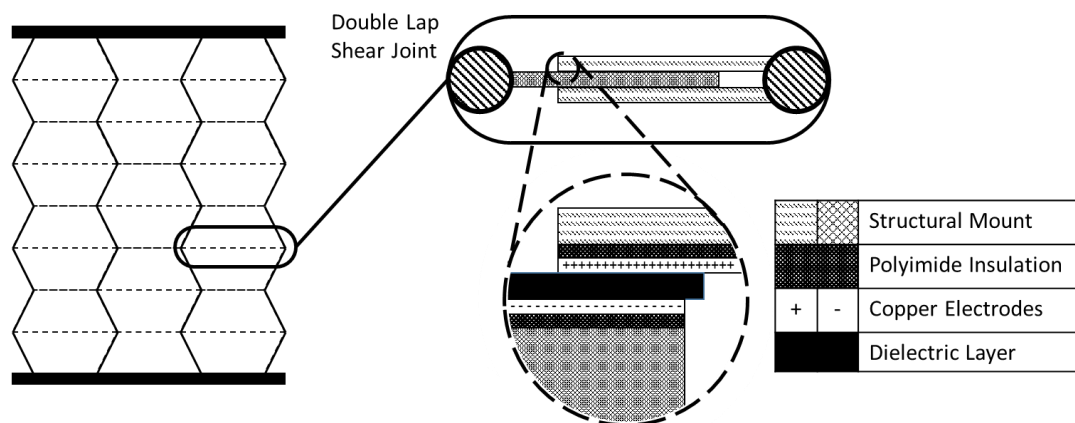
8   FIGURES

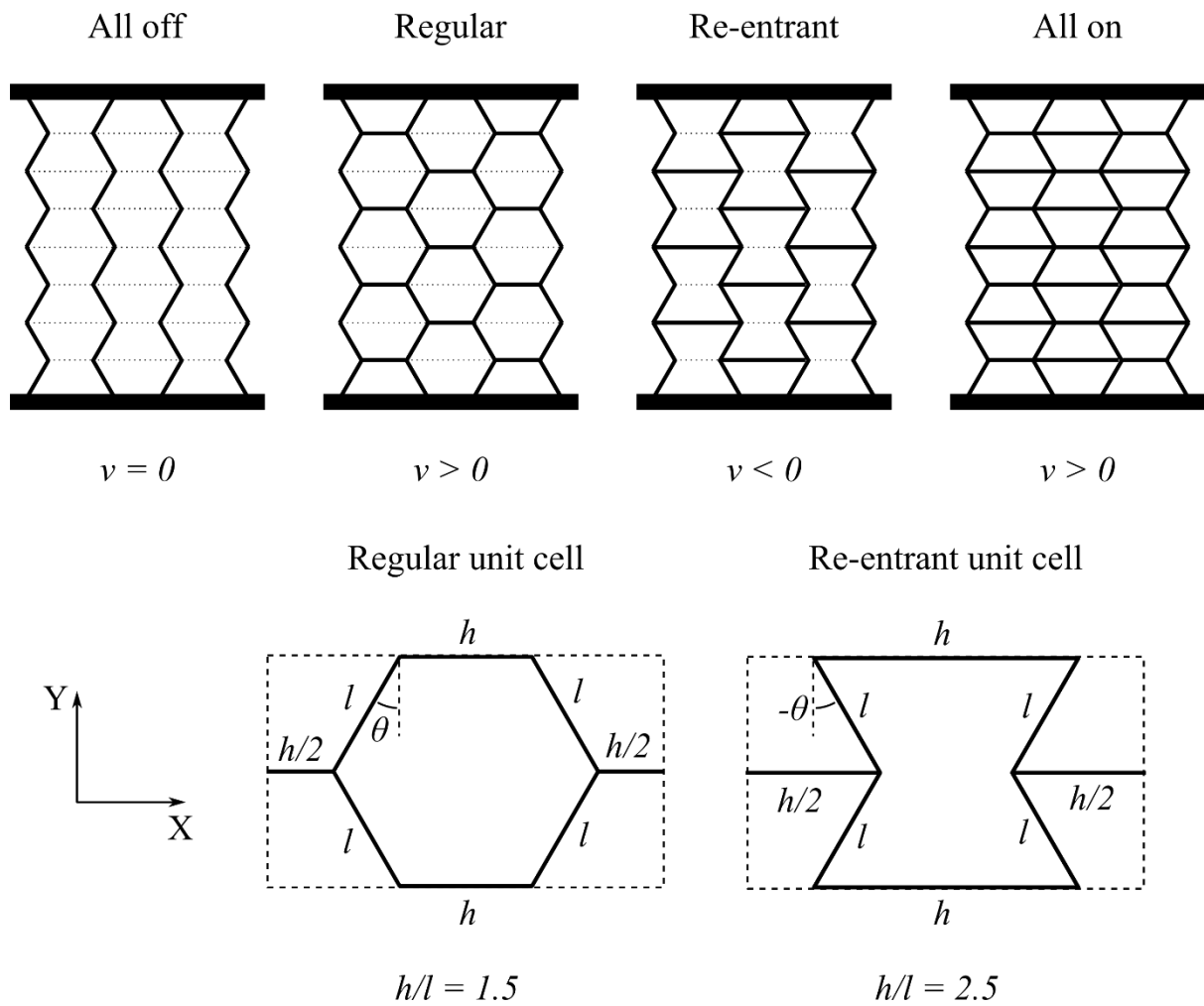Figure 1: Introducing Electrostatic adhesive elements to a cellular structure.

Figure 2: Possible configurations of the cellular array (top) and unit cells of the regular and re-entrant configurations (bottom). Note that θ is negative for the re-entrant cell.
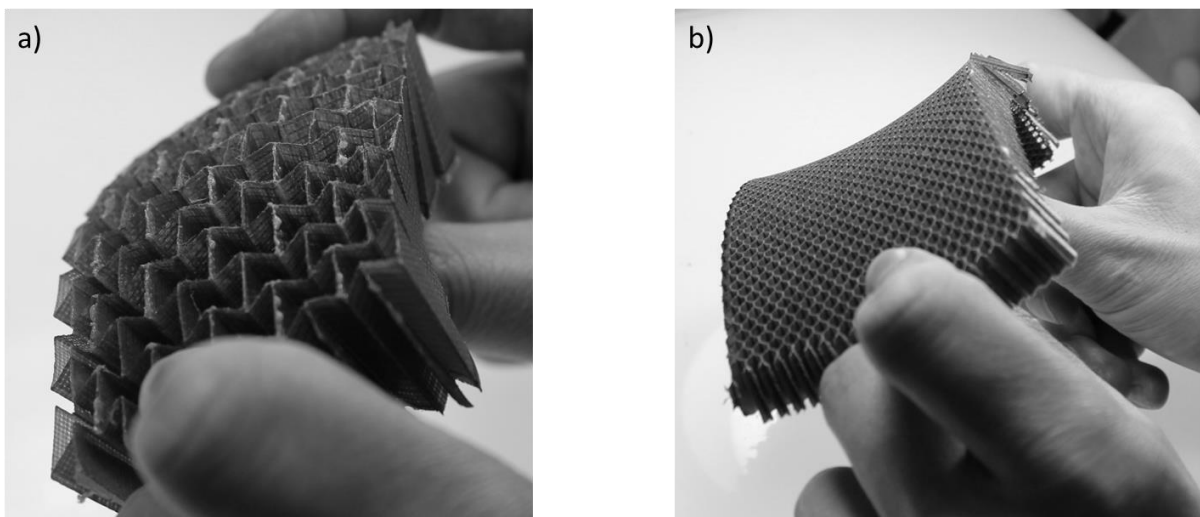

Figure 3: Secondary curvature caused by Poisson's ratio. (a) Synclastic curvature caused by negative Poisson's ratio. (b) Anticlastic curvature caused by positive Poisson's ratio.
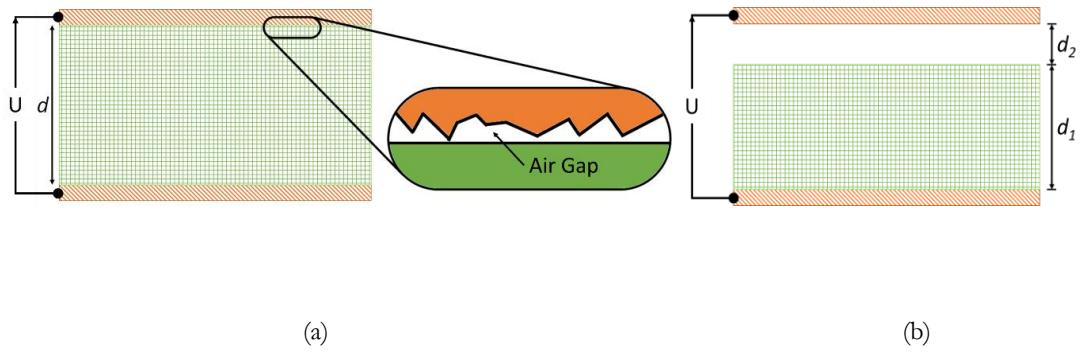
Figure 4: (a) Initially assumed electrode configuration and air gap existence (U = applied voltage, d = dielectric thickness) (b) Representation of electrode configuration accounting for an included air gap (d_1 = dielectric thickness d_2 = air gap thickness).
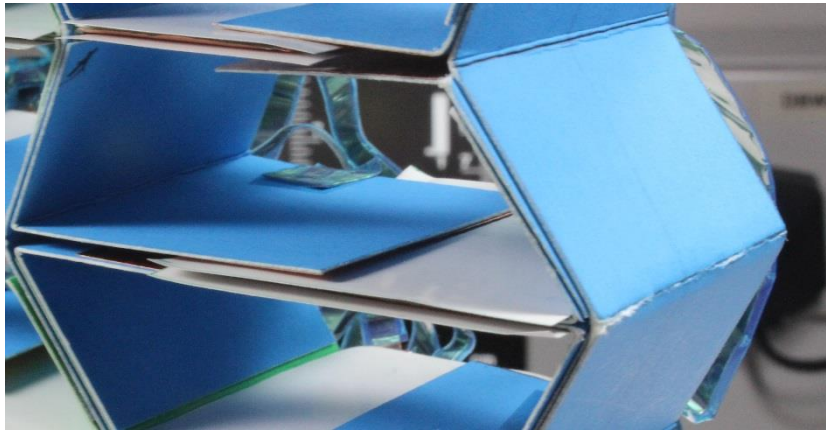
Figure 5: Close up of interlocking electroadhesive joints (as in Figure 1).

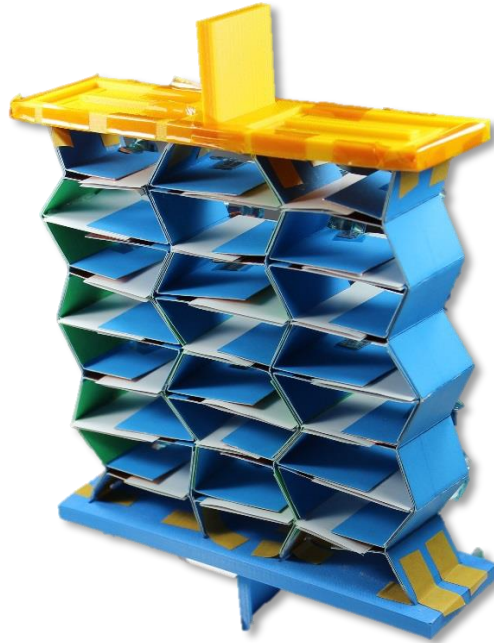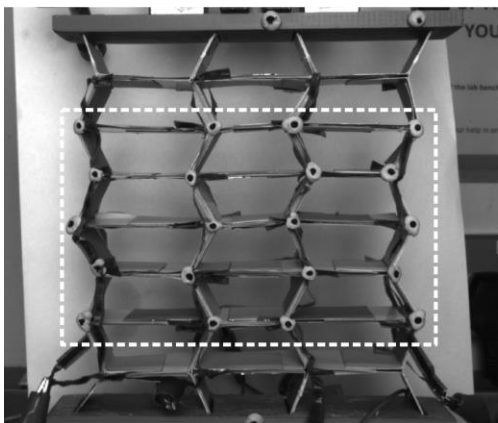Figure 6: Individual Column Elements of Cellular Structure.
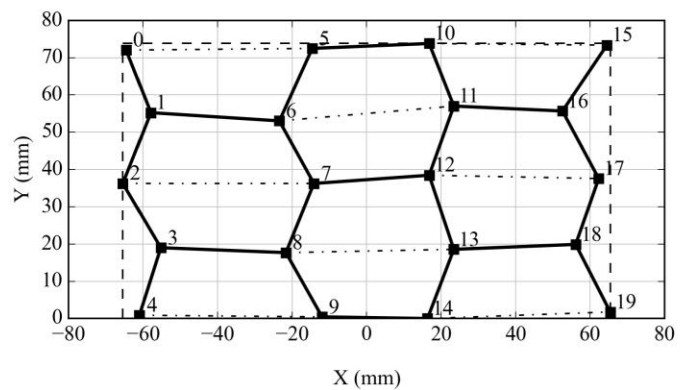
Figure 7: Completed prototype attached to end tabs.

a)   b)

Figure 8: Video gauge strain measurement. a) Still frame from the video gauge recording, showing the location of targets for the video gauge system. b) Virtual representation of the honeycomb based on the targets' XY coordinates.
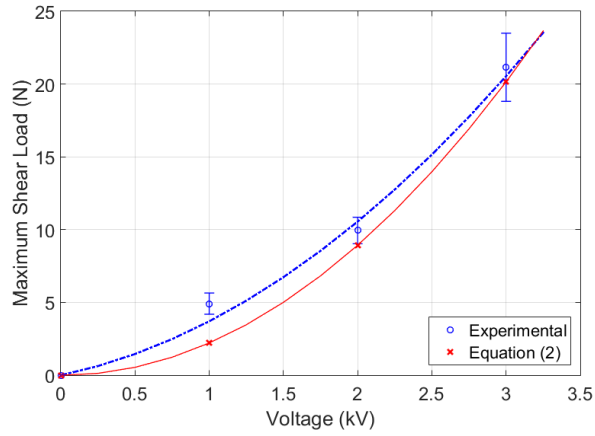
Figure 9: Electrostatic shear holding force at each double lap shear joint.

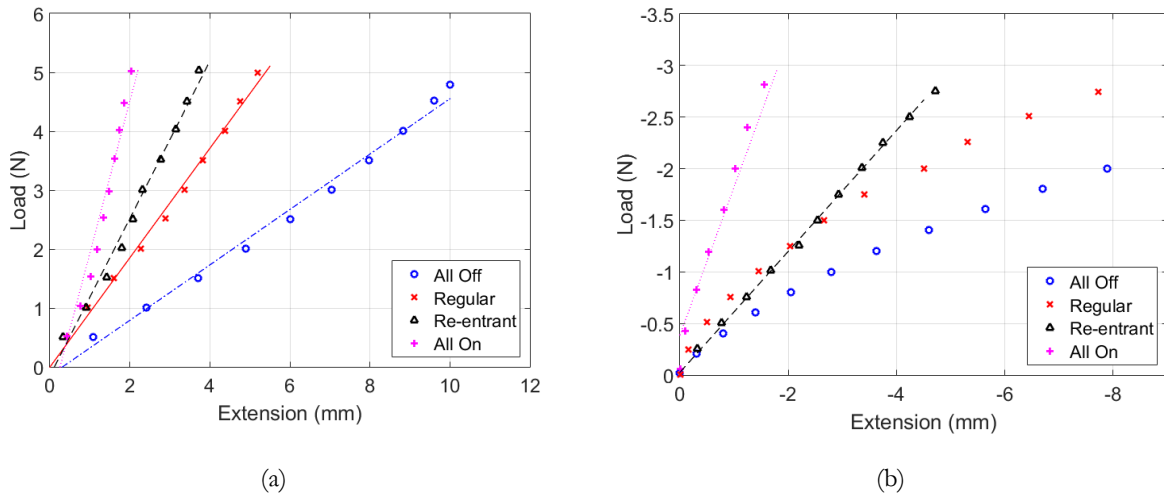(a)   (b)

Figure 10: Load-Extension curves (a) Tensile Loading (b) Compressive Loading ('All Off' and Regular highly non-linear. Linear curve approximations thus omitted)
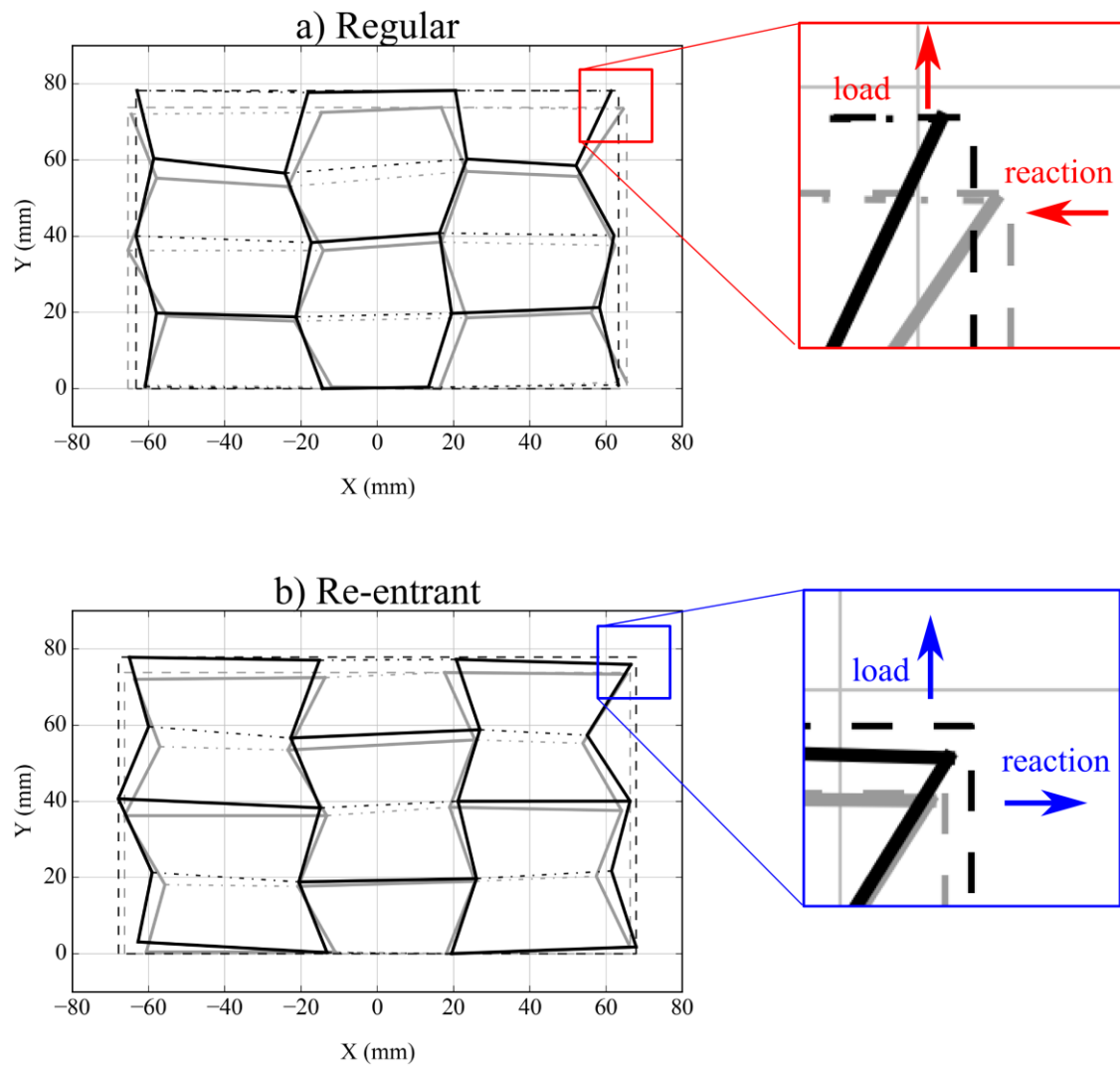
Figure 11: Honeycomb vertex locations for the initial position ($\Delta y = 0$ mm – grey line) and the final position ($\Delta y = 4$ mm – black line). (a) and (b) show the two configurations. The insets show a closer view of the specimen corners to make the Poisson's ratio behaviour more easily observable.
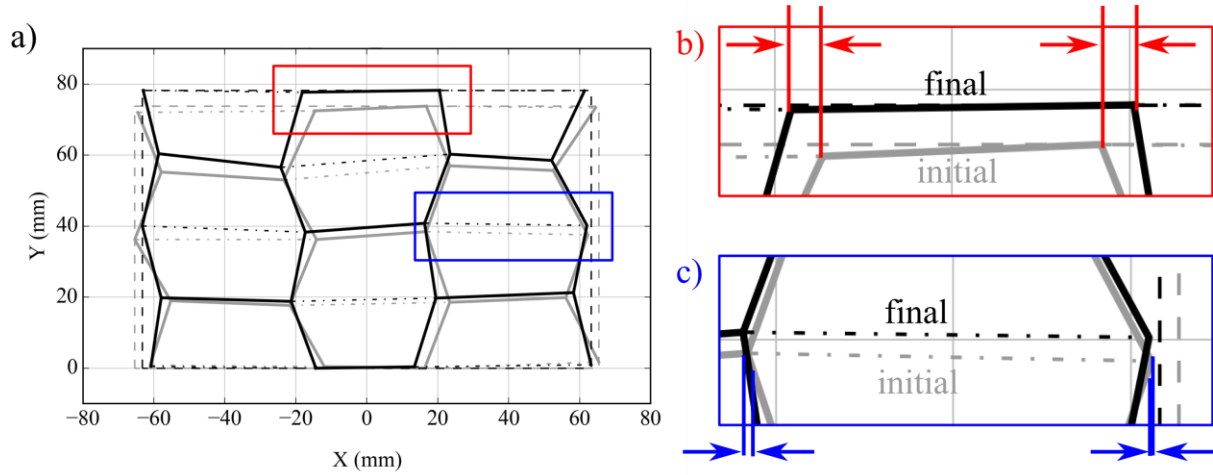
Figure 12: Examples of defects in the regular honeycomb structure, as observed in the video gauge data. (a) Shows the regular cellular structure at $\Delta y = 0$ mm (grey lines) and $\Delta y = 4$ mm (black lines). (b) Shows an activated linkage change in length – i.e. an example of slippage. (c) Shows a deactivated linkage remaining the same length when we expect it to contract – i.e. an example of unintentional sticking.

9   TABLES

Table 1: Example values of electrostatic holding strengths for given parameter values.

Voltage (kV)	Air Gap (μm)	Normal Adhesive Strength (MPa)	Shear Traction	
			Single Lap (MPa)	Double Lap (MPa)
2	2	0.038	0.008	0.016
3	2	0.085	0.017	0.034
2	3.5	0.025	0.005	0.010
3	3.5	0.056	0.011	0.022

Table 2: Cell dimensions.

Dimension	Regular configuration		Re-entrant configuration	
h	30	mm	50	mm
l	20	mm	20	mm
b	15	mm	15	mm
θ	30	°	-30	°

Table 3: Theoretical Poisson's ratios.

	Regular	Re-entrant
ν_{xy}	1.333	-1.333
ν_{yx}	0.75	-0.75

Table 4: Cellular Stiffness Comparisons.

Cellular Configuration	Tensile Loading		Compressive Loading	
	Equivalent Stiffness (N/mm)	% Changes	Equivalent Stiffness (N/mm)	% Changes
All Off	0.4701	0 %	0.2442	0 %
Regular	0.9285	98 %	0.3126	28 %
Re-entrant	1.3359	184 %	0.5561	128 %
All On	2.5833	450 %	1.4357	488 %

Table 5: Overall geometry approximations and Poisson's ratio

| Configuration	Start Width (mm)	Start Height (mm)	Δx (mm)	Δy (mm)	ϵ_x (-)	ϵ_y (-)	ν_{xy} (-)	ν_{yx} (-)
Regular	130.81	73.80	-4.29	4.46	-0.0327	0.0604	1.84	0.54
Re-entrant	132.58	73.81	3.23	4.01	0.0243	0.0543	-2.23	-0.45
All on	125.6	72.5	-2.60	4.01	-0.0207	0.0553	2.67	0.37

REFERENCES

[1]   Tabata O, Konishi S, Cusin P, Ito Y, Kawai F, Hirai S and Kawamura S Microfabricated tunable bending stiffness device *Proceedings IEEE Thirteenth Annual International Conference on Micro Electro Mechanical Systems (Cat. No.00CH36308)* 23–7

[2]   Bergamini A, Christen R, Maag B and Motavalli M 2006 A sandwich beam with electrostatically tunable bending stiffness *Smart Materials and Structures* **15** 678–86

[3]   Bergamini A, Christen R and Motavalli M 2007 Electrostatically tunable bending stiffness in a

GFRP–CFRP composite beam *Smart Materials and Structures* **16** 575–82

[4]   Bergamini A 2009 *Electrostatic modification of the bending stiffness of adaptive structures* (ETH)

[5]   Heath C J C, Bond I P and Potter K D 2016 Electrostatic adhesion for added functionality of composite structures *Smart Materials and Structures* **25** 11

[6]   Di Lillo L, Raither W, Bergamini A, Zündel M and Ermanni P 2013 Tuning the mechanical behaviour of structural elements by electric fields *Applied Physics Letters* **102** 224106

[7]   Raither W, Furger E, Zündel M, Bergamini A and Ermanni P 2013 Variable-stiffness skin concept for camber-morphing airfoils *24th International Conference on Adaptive Structures Technologies (ICAST2013)* 1–14

[8]   Raither W, Simoni L De and Lillo L Di 2014 Adaptive-Twist Airfoil Based on Electrostatic Stiffness Variation *AIAA SciTech*

[9]   Lakes R 1987 Foam structures with a negative Poisson's ratio *Science* **235** 1038–40

[10]   Lakes R 1991 Deformation mechanisms in negative Poisson's ratio materials: structural aspects *Journal of Materials Science* **26** 2287–92

[11]   Evans K 1991 The design of doubly curved sandwich panels with honeycomb cores *Composite Structures* **17** 95–111

[12]   Evans K E, Nkansah M A, Hutchinson I J and Rogers S C 1991 Molecular Network Design *Nature* **353** 124

[13]   Bitzer T 1997 *Honeycomb technology - materials, design, manufacturing, applications and testing* (London: Chapman & Hall)

[14]   Gibson L J and Ashby M F *Cellular Solids: Structure and properties* (Cambridge University Press)

[15]   Masters I G and Evans K E 1996 Models for the elastic deformation of honeycombs *Composite Structures* **35** 403–22

[16]   Prall D and Lakes R S 1997 Properties of a chiral honeycomb with a poisson's ratio of — 1 *International Journal of Mechanical Sciences* **39** 305–14

[17]   Grima J N, Oliveri L, Attard D, Ellul B, Gatt R, Cicala G and Recca G 2010 Hexagonal honeycombs with zero Poisson's ratios and enhanced stiffness *Advanced Engineering Materials* **12** 855–62

[18]   Grima J N and Attard D 2011 Molecular networks with a near zero Poisson's ratio *Physica Status Solidi (B)* **248** 111–6

[19]   Olympio K and Gandhi F 2007 Zero-ν cellular honeycomb flexible skins for one-dimensional wing morphing *48th Structures, Structural Dynamics, and Materials Conference, AIAA/ASME/ASCE/AHS/ASC, Honolulu, Hi. April* 23–6

[20]   Olympio K R and Gandhi F 2010 Zero Poisson's Ratio Cellular Honeycombs for Flex Skins Undergoing One-Dimensional Morphing *Journal of Intelligent Material Systems and Structures* **21** 1737–53

[21]   Lira C, Scarpa F, Olszewska M and Celuch M 2009 The SILICOMB cellular structure: Mechanical and dielectric properties *Physica Status Solidi (B) Basic Research* **246** 2055–62

[22]   Lira C, Scarpa F L, Tai Y H and Yates J R 2011 Transverse shear modulus of SILICOMB cellular structures *Composites Science and Technology* **71** 1236–41

[23]   Virk K, Monti A, Trehard T, Marsh M, Hazra K, Boba K, Remillat C D L, Scarpa F and Farrow I R 2013 SILICOMB PEEK Kirigami cellular structures: mechanical response and energy dissipation through zero and negative stiffness *Smart Materials and Structures* **22** 084014

[24]   Chen Y, Scarpa F, Remillat C, Farrow I, Liu Y and Leng J 2013 Curved Kirigami SILICOMB cellular structures with zero Poisson's ratio for large deformations and morphing *Journal of Intelligent Material Systems and Structures* **0** 1–13

[25]   Neville R M, Monti A, Hazra K, Scarpa F, Remillat C and Farrow I R 2014 Transverse stiffness and strength of Kirigami zero-ν PEEK honeycombs *Composite Structures* **114** 30–40

[26]   Huang J, Gong X, Zhang Q, Scarpa F, Liu Y and Leng J 2016 In-plane mechanics of a novel zero Poisson's ratio honeycomb core *Composites Part B: Engineering* **89** 67–76

[27]   Gong X, Huang J, Scarpa F, Liu Y and Leng J 2015 Zero Poisson's ratio cellular structure for two-dimensional morphing applications *Composite Structures* **134** 384–92

[28]   Mao J, Qin L and Wang Y 2014 Modeling and simulation of electrostatic attraction force for climbing robots on the conductive wall material *2014 IEEE International Conference on Mechatronics and Automation (ICMA)* (IEEE) pp 987–92

[29]   Du Pont DuPont Tedlar Polyvinyl Flouride (PVF) Films General Properties *http://www.dupont.com/content/dam/dupont/products-and-services/membranes-and-films/pvf-films/documents/DEC_Tedlar_GeneralProperties.pdf*
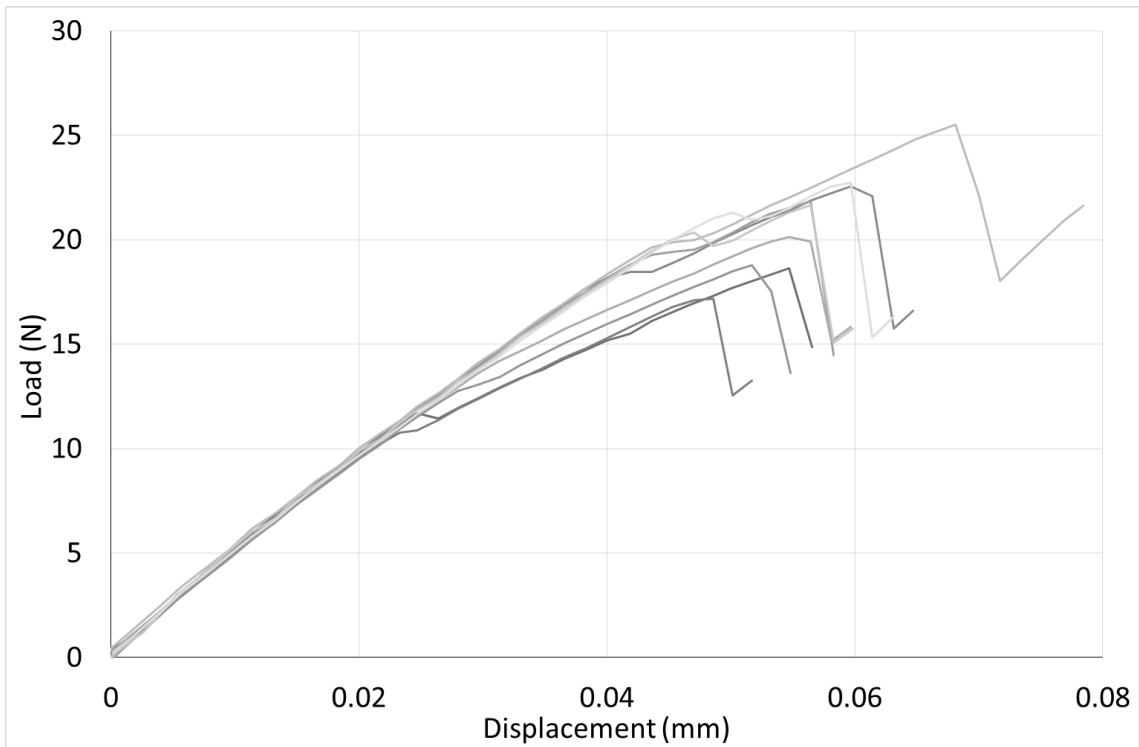
APPENDIX
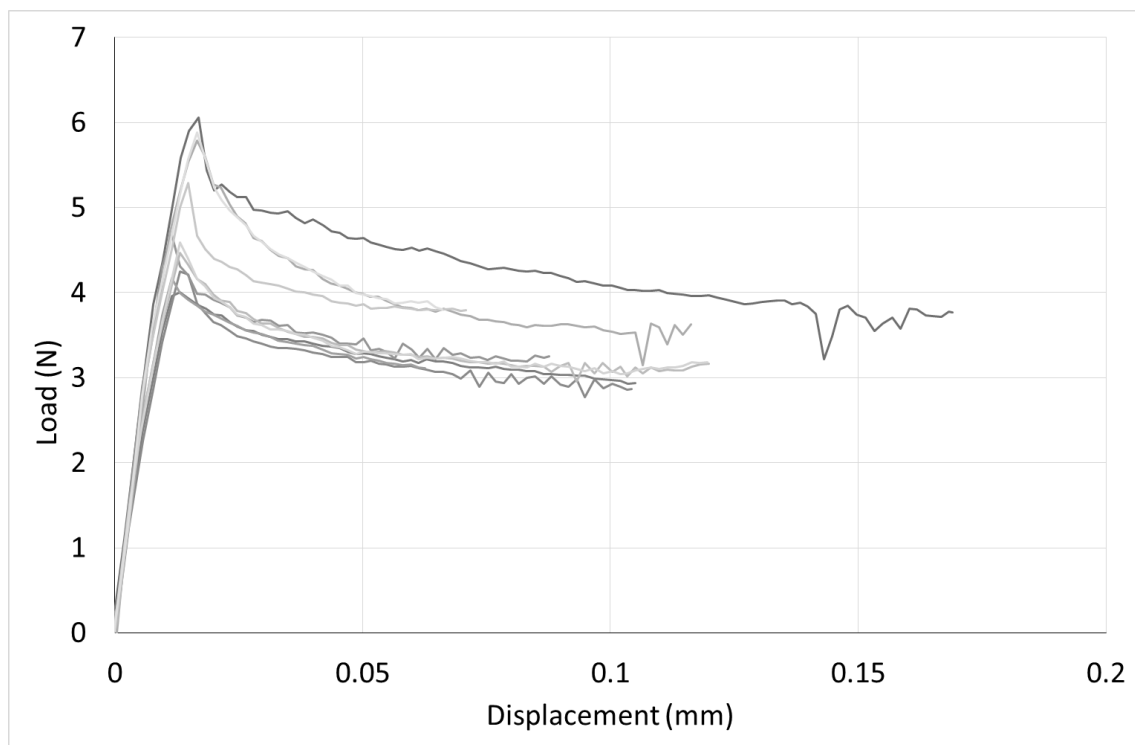
A1: 1 kV electrostatic adhesion test data
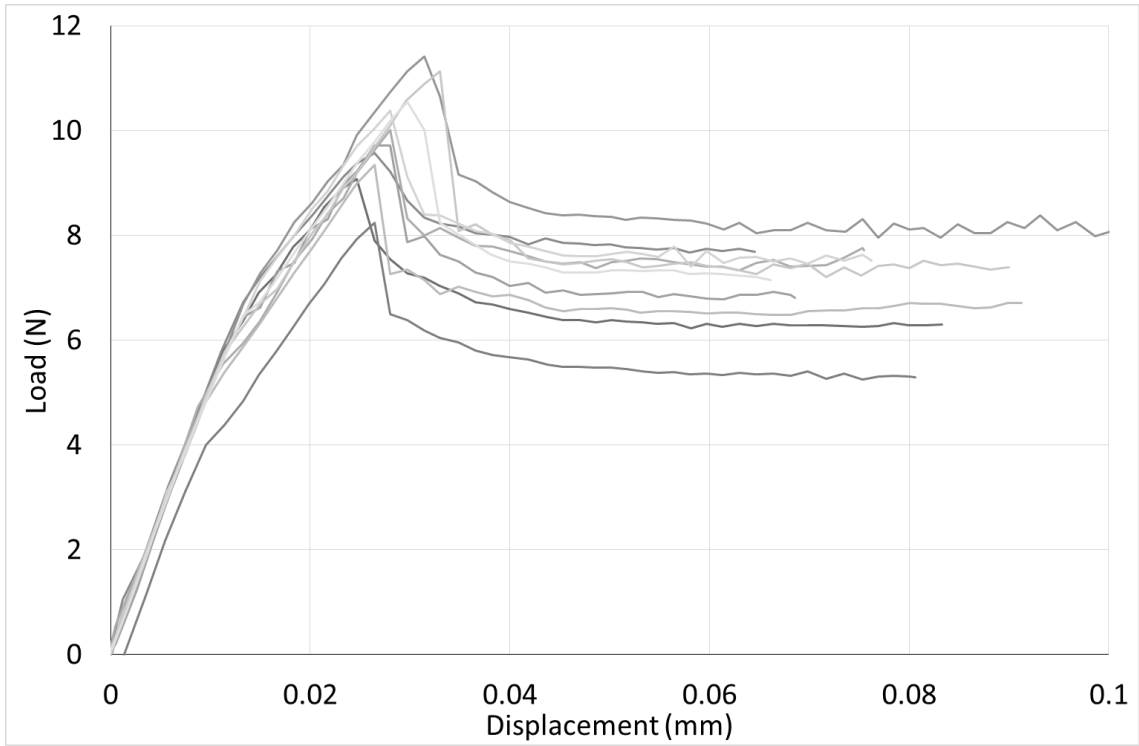
A2: 2 kV electrostatic adhesion test data

A3: 3 kV electrostatic adhesion test data